



## Hybrid CaCO<sub>3</sub>-mucin crystals: Effective approach for loading and controlled release of cationic drugs

Nadezhda G. Balabushevich<sup>a</sup>, Ekaterina A. Kovalenko<sup>a</sup>, Irina M. Le-Deygen<sup>a</sup>, Lyubov Y. Filatova<sup>a</sup>, Dmitry Volodkin<sup>a,b</sup>, Anna S. Vikulina<sup>b,c,\*</sup>

<sup>a</sup> Lomonosov Moscow State University, Department of Chemistry, Leninskiye Gory 1-3, 119991 Moscow, Russia

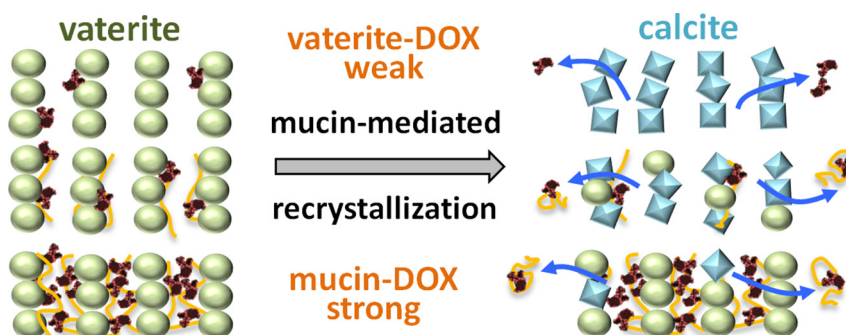
<sup>b</sup> Nottingham Trent University, School of Science and Technology, Clifton Lane, NG11 8NS Nottingham, UK

<sup>c</sup> Fraunhofer Institute for Cell Therapy and Immunology, Branch Bioanalytics and Bioprocesses, Am Mühlenberg 13, 14476 Potsdam-Golm, Germany

### HIGHLIGHTS

- Co-loading of mucin and doxorubicin into vaterite crystals enhances doxorubicin content by ca 12 times.
- At pH 7.4, doxorubicin-mucin complex release is driven by the recrystallization of the porous vaterite to non-porous calcite.
- Degree of recrystallization can be controlled via the content of mucin in hybrid crystals.

### GRAPHICAL ABSTRACT



### ARTICLE INFO

#### Article history:

Received 1 April 2019

Received in revised form 4 July 2019

Accepted 5 July 2019

Available online 06 July 2019

#### Keywords:

Vaterite

Co-synthesis

Doxorubicin

Aprotinin

Prolonged release

Mucosal delivery

### ABSTRACT

Vaterite CaCO<sub>3</sub> crystals are actively used as a biocompatible and degradable matrix for encapsulation of fragile biomacromolecules. However, the incorporation of small cationic drugs into the crystals remains awkward due to a poor binding of these drugs to the crystal surface and scarce retention inside the crystal pores. Herein, we achieve efficient drug loading and control over drug release performance via utilisation of hybrid CaCO<sub>3</sub> crystals impregnated with mucin. The co-loading of mucin and anticancer drug doxorubicin (DOX) into CaCO<sub>3</sub> crystals enhanced drug content in the crystals by ca 12 times giving DOX concentration of 1.3 mg g<sup>-1</sup> CaCO<sub>3</sub>. Retention of DOX inside hybrid crystals is governed by strong electrostatic attraction to mucin matrix and significant narrowing of the crystal pores in the presence of mucin. At physiologically relevant conditions, DOX release kinetics strongly depends on the recrystallization of the porous vaterite to non-porous calcite that is regulated by mucin concentration. We believe that this study will help to design novel effective drug delivery systems able to load high amounts of drugs at mild conditions for sustained and controlled release of the drugs. This is indispensable for mucosal delivery where mucin produced by epithelial tissues is a main component.

© 2019 The Authors. Published by Elsevier Ltd. This is an open access article under the CC BY-NC-ND license (<http://creativecommons.org/licenses/by-nc-nd/4.0/>).

\* Corresponding author at: Fraunhofer Institute for Cell Therapy and Immunology, Branch Bioanalytics and Bioprocesses, Am Mühlenberg 13, 14476 Potsdam-Golm, Germany. E-mail addresses: [dmitry.volodkin@ntu.ac.uk](mailto:dmitry.volodkin@ntu.ac.uk) (D. Volodkin), [anna.vikulina@izi-bb.fraunhofer.de](mailto:anna.vikulina@izi-bb.fraunhofer.de) (A.S. Vikulina).

## 1. Introduction

Nowadays nano- and micro-crystals of  $\text{CaCO}_3$  are extremely attractive as vectors for direct loading and controlled release of biologically active molecules as well as decomposable matrices for hard templating of polymer-based particles [1–6].

Vaterite polymorph of  $\text{CaCO}_3$  is of special interest [1] because it can be easily synthesized in laboratory from inexpensive precursor salts (e.g.  $\text{CaCl}_2$  and  $\text{Na}_2\text{CO}_3$ ) yielding crystals of adjustable dimensions ranging from hundreds of nanometres up to tens of micrometres. In addition to biocompatibility, the vaterite crystals are mesoporous, i.e. have pore sizes in the range of tens of nanometres that allows effectively hosting and protecting both small compounds (e.g. antibiotics, anticancer and other drugs [7], nanoparticles [8]) and rather large biomacromolecules (proteins [9–11], hormones [12], enzymes [13], RNA [14]). Besides the dimensions, porosity [15] and the shape of the crystals [16] can be modulated in a broad range, accordingly to the area of applications of the crystals.

The crystals can serve as sacrificial templates to assemble multilayer capsules [17], macrostructures such as scaffolds [18–21] as well as porous particles made of biologically relevant functional molecules such as polyethylene glycol and poly-*N*-isopropylacrylamide [22,23]. The crystals have been employed as tailor-made matrices for diagnostics, e.g. using Raman spectroscopy [24,25], and can be functionalised providing external control over drug release [26]. Vaterite  $\text{CaCO}_3$  crystals can be multifunctional in regards with their role as templates, e.g. they can serve as porogens and a source of calcium to assemble porous alginate gels with biomolecules loaded into the pores [27,28].

Both low- and high-molecular-weight bioactives have been successfully encapsulated into the vaterite crystals, yet negatively charged proteins can be loaded into crystals in significantly high amounts [29], whereas positively charged bioactives can scarcely be loaded in substantial amounts and are quickly released from the crystals upon washing. This has been demonstrated for protamine and aprotinin (APR) [29], lysozyme [30] and doxorubicin (DOX) [31].

A number of synthetic polymers added during the growth of  $\text{CaCO}_3$  crystals can affect morphology and thermodynamic state of the crystals: poly(sodium 4-styrene-sulfonate), poly(allylamine hydrochloride), poly(acrylic acid), poly(vinyl alcohol), polyacrylamide, poly(*N*-isopropyl acrylamide), poly(*N*-vinyl pyrrolidone), poly(ethylene oxide), carboxymethyl cellulose [32–34]. Biopolymers such as pectin, carrageenan, alginate, chitosan, xanthan, hyaluronic acid, heparin have been reported to affect the crystal properties [32,33]. In spite of significant influence of the polymers on the crystal properties and structure, the formulation of polymer-containing hybrid crystals may open new ways for the encapsulation of the molecules of interest via their binding to the polymer matrix. Some examples for such two-component vaterite crystals have been recently reported. For instance, carrageenan- $\text{CaCO}_3$  crystals can host DOX and release the drug in a sustained manner [31]. Recently, DOX-loaded hyaluronate calcium carbonate hybrid nanoparticles have been successfully designed for the inhibition of the tumour [35]. Similarly to small drugs like DOX, protein-based drugs have been encapsulated into polymer-containing vaterite crystals: heparin- $\text{CaCO}_3$  hybrids can host large amount of lysozyme and keep it during layer-by-layer coating of the crystal [30], the matrices of silane-coupling polymers facilitate the retention of cisplatin (one of the most successful chemotherapeutics) [36].

In recent years, a surge of interest to the loading of the vaterite crystals with mucoadhesive biopolymers such as mucin has emerged to employ the crystals for drug delivery in mucosa [7,37]. Mucins are the main components of mucous membranes in the gastrointestinal tract, as well as nasal and oral mucous membranes [38]. These large extracellular glycoproteins have molecular weights ranging from 0.5 to 20 MDa. Mucins are classified as membrane-bound and secreted mucins and both types share many common features [39]. They consist of 80% carbohydrates which are mainly *N*-acetylgalactosamine, *N*-acetylglucosamine, fucose,

galactose, and sialic acid (*N*-acetylneuraminic acid); remaining 20% constitute the protein core. The oligosaccharide chains built up of 5–15 simple sugars are attached to the hydroxyl side chains of serine and threonines of so called central glycosylated region of the protein core which is comprised of multiple tandem repeats rich in serine, threonine, and proline (STP repeats). At the amino and carboxy terminals, as well as between STP repeats, there are regions of the second type that is called cysteine-rich domain as the content of cysteine in these regions is >10%. Disulfide bonds formed between cysteine-rich domains of neighbouring mucin molecules lead to subsequent dimerization and polymerization of glycoprotein. Due to this structure a number of various interactions are present in mucins including electrostatics, hydrophobic interactions, and hydrogen bonding; these interactions largely define the properties of mucins (Fig. 1). In our previous paper we have demonstrated loading of mucin into the vaterite crystals via physisorption [40] and co-synthesis at low concentrations below  $1 \text{ mg mL}^{-1}$  [37]. These studies demonstrated a high promise for the use of mucin-containing formulations for drug delivery via mucosa; now we address the challenge of the design of hybrid drug delivery systems for effective delivery of small cationic drugs in a sustained manner.

In present work, we develop novel mucin-containing vaterite crystals for effective loading and controlled release of small cationic drugs. We have utilized DOX - a drug that is widely used in therapy of numerous cancers. DOX formulations are widely used via oral and intravenous administrations into cervical [41] and lung carcinoma [42,43], primary and metastatic melanoma [44], osteosarcoma [45] and hepatoma [46], providing long-term release performance [14,47–49], however limited intestinal absorption of DOX via mucosal surfaces is not yet fully circumvented [48]. In addition to DOX, loading and release of two protein-based therapeutics (protease inhibitor aprotinin and hormone insulin), are also investigated. We discuss on fundamentals of the  $\text{CaCO}_3$  biomineralization and potential of hybrid crystals for controlled drug delivery.

## 2. Experimental section

### 2.1. Materials

Anhydrous calcium chloride,  $\geq 93.0\%$  (C1016), anhydrous sodium carbonate  $\text{Na}_2\text{CO}_3$ ,  $\geq 99.0\%$  (S7795), commercial mucin from porcine stomach, Type III, (m1778), aprotinin, *N*-benzoyl-L-arginine ethyl ester, *N*-acetylneuraminic acid from *E. coli* (Sigma-Aldrich, USA); trypsin from bovine pancreas (Fluka, Germany); doxorubicin hydrochloride substance (Dian Jiang Chong, China). Human recombinant insulin zinc salt was kindly provided by the Experimental Biotechnology Plant of Shemyakin–Ovchinnikov Institute of Bioorganic Chemistry, Russian Academy of Sciences. All chemicals for buffer solutions were laboratory grade and purchased from Sigma–Aldrich, USA. Before use, mucin solutions were sonicated for 30 min using the ultrasonic bath (Elmasonic S15H, Germany).

### 2.2. Analytical determination of mucin and drugs

The concentration of DOX in the solutions was determined spectrophotometrically at 480 nm ( $\epsilon = 12,500 \text{ M}^{-1} \text{ cm}^{-1}$ ) [50]. The concentration of active aprotinin in the solutions was determined by inhibition of trypsin using BAEE substrate as described [51,52]. In the study of adsorption isotherms, the concentration of the mucin in solution was determined spectrophotometrically at the wavelengths of 260 nm. In all other experiments concentration of mucin and insulin in solution were determined by analytical size exclusion chromatography [37] in the Biofox 17 SEC 8  $\times$  300 mm column (Bio-Works, Sweden) using the Smartline chromatographic system (Knauer, Germany) in a solution of 0.15 M NaCl. Preliminarily, the column was calibrated using solutions of purified mucin and insulin with different concentrations (0.01–0.1  $\text{mg mL}^{-1}$ ) and proteins with different molecular weights. A

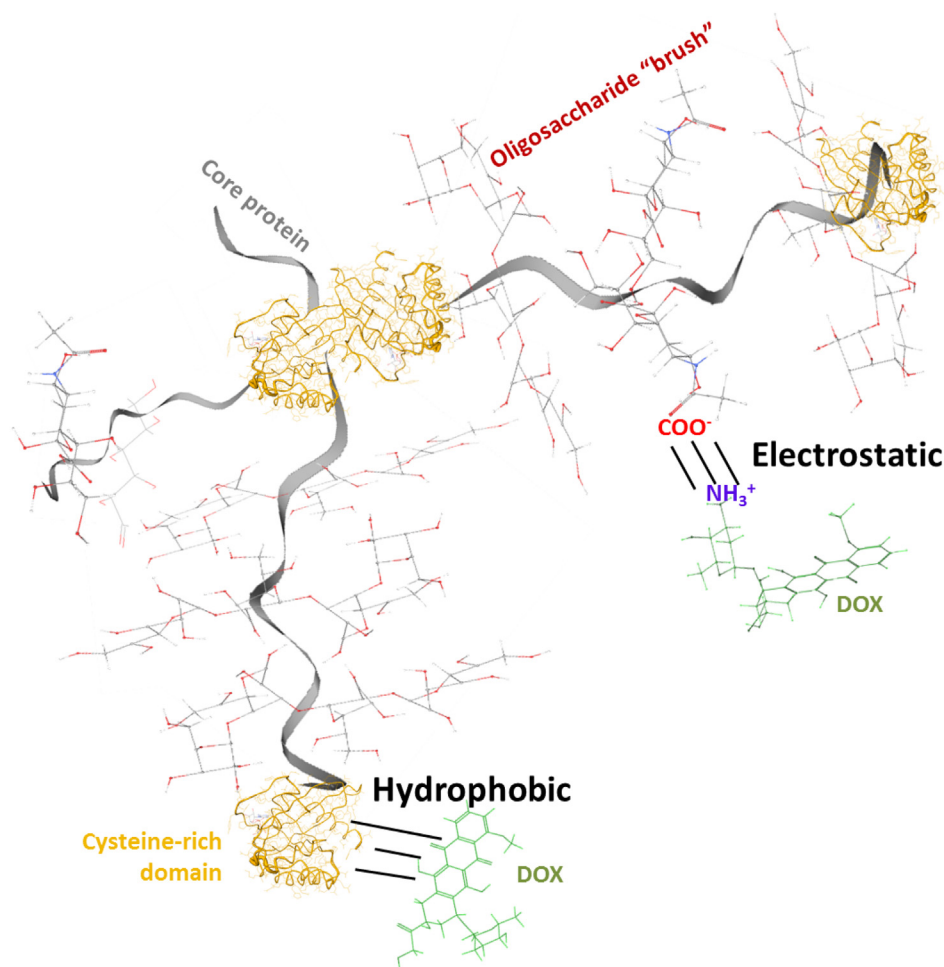


Fig. 1. Schematic structure of mucin and its mucoadhesive elements highlighting potential sites for mucin-DOX interaction.

total of 0.2 mL of the mucin or insulin solution was used for the chromatography analysis at the elution rate of 0.5 mL min<sup>-1</sup>. Absorbance of the eluted solutions was measured using the UV detector at wavelengths of 214 nm and 260 nm.

The content of sialic acids in mucin, determined by Hess's method using the calibration curve for *N*-acetylneuraminic acid and was found to be 2.30 ± 0.10% [37].

### 2.3. Preparation and characterization of the CaCO<sub>3</sub>-mucin-drug hybrids

3 mL of the solution (water or 0.05 M TRIS buffer, pH 7.1) containing 0.167–10 mg mL<sup>-1</sup> mucin and/or 1.67 mg mL<sup>-1</sup> protein (APR/INS) or 0.167 mg mL<sup>-1</sup> DOX were added to 1 mL of the solution 1 M CaCl<sub>2</sub>. The solution was stirred for 5 min (100 rpm). 1 mL of the solution of 1 M Na<sub>2</sub>CO<sub>3</sub> was added and further stirred for an additional 45 s. Then the suspension was incubated for 15 min. The precipitate was separated by centrifugation (2 min, 1000 g) and washed twice with 5 mL of water. If necessary, the particles were dried. The mass of the precipitate was determined, and the mass of CaCO<sub>3</sub> was calculated assuming the complete process of crystallization of the insoluble crystals. The concentrations of mucin and drug were determined in the supernatant and washing solutions.

The amount of adsorbed mucin saturation conditions (equilibrium) was calculated using the following equation:

$$q_e = \frac{(C_0 - C_e) \cdot V}{m} \quad (1)$$

where  $q_e$  is the adsorption capacity (mg g<sup>-1</sup>),  $C_0$  and  $C_e$  are the initial and equilibrium concentrations (mg mL<sup>-1</sup>);  $V$  is the volume (mL) of the solution; and  $m$  is the mass (mg) of CaCO<sub>3</sub>.

Efficiency of mucin or drug incorporation was calculated using the equation:

$$\eta = \frac{C_0 - C_e}{C_0} \quad (2)$$

The isotherm for mucin loading via co-synthesis (initial mucin concentration 0.1–6 mg mL<sup>-1</sup>) has been constructed based on Langmuir adsorption model according to the Langmuir equation below:

$$q_e = \frac{q_{max} K_a C_e}{1 + K_a C_e} \quad (3)$$

where  $q_e$  – equilibrium adsorption capacity (mg g<sup>-1</sup>);  $C_e$  – concentration of mucin in the solution at equilibrium (mg mL<sup>-1</sup>);  $q_{max}$  – maximum adsorption capacity (mg g<sup>-1</sup>);  $K_a$  – adsorption equilibrium constant (mL mg<sup>-1</sup>).

The free Gibbs energy ( $\Delta G$ ) has been calculated as  $-RT \ln K_a$ , where  $R$  is the universal gas constant, 8.31 (J K<sup>-1</sup> mol<sup>-1</sup>);  $T$  is the temperature (K);  $K_a$  is the constant of adsorption equilibrium in units of L mol<sup>-1</sup>.

### 2.4. Study of drug release

The centrifuged precipitate of the CaCO<sub>3</sub> crystals was combined with 5 mL 0.05 M TRIS buffer, pH 7.4. The suspension was continuously

stirred (100 rpm, 37 °C). After 1, 3, 6, and 24 h, aliquots were taken, centrifuged (2 min, 10,000 g), and analyzed. The mucin or drug release was estimated by the ratio of the concentrations of the supernatant and suspension.

### 2.5. Microscopy analysis

CaCO<sub>3</sub> crystals were visualized using an optical microscope Carl Zeiss, JENA (Germany) to get transmission light images. Scanning electron microscopy (SEM) images were recorded using a Gemini LEO 1550 electron microscope at an accelerating voltage of 3 kV. Samples were prepared by dropping the crystal suspension on a glass slide, dried within 1 h at 90 °C and followed by conductive coating with gold palladium (5 nm).

### 2.6. $\zeta$ -potential measurement

The  $\zeta$ -potential of CaCO<sub>3</sub> crystals and mucin was measured using Zetasizer (Nano ZS, Malvern, UK) and estimated using Smoluchowski eq.

### 2.7. ATR-FTIR spectroscopy

ATR-FTIR spectra were recorded using a Bruker Tensor 27 spectrometer equipped with a liquid nitrogen cooled MCT (mercury cadmium telluride) detector. Samples were placed in a thermostatic cell BioATR-II with a ZnSe ATR element (Bruker). The FTIR spectrometer was purged with a constant flow of dry air. FTIR spectra were acquired from 900 to 3000 cm<sup>-1</sup> with 1 cm<sup>-1</sup> spectral resolution. For each spectrum, 100 scans were accumulated at 20 kHz scanning speed and averaged. All samples were prepared in aqueous buffer solution using deionized water at 22 °C. Spectral data were processed using the Bruker software Opus 7.5 as described elsewhere [53–55], which includes linear blank subtraction, straight-line baseline correction and atmosphere compensation. If necessary, seven- or nine-point Savitsky–Golay smoothing was used to remove white noise. The peaks were identified by standard Bruker picking-peak procedure.

Solid-phase ATR-FTIR spectroscopy of lyophilized precipitates was conducted with Vertex 70 V Bruker machine (Germany) equipped with PLATINUM ATR diamond cell. Spectra were registered with 4 cm<sup>-1</sup> resolution from 4000 cm<sup>-1</sup> to 350 cm<sup>-1</sup>, 24 scans for each spectrum. Spectra were analyzed with Bruker Opus 7.0 software.

### 2.8. X-ray diffraction spectroscopy (XRD)

X-ray powder diffraction analysis was performed using a Bruker D8 Advance X-ray powder diffractometer with a silicon drift detector on powdered samples using Cu Ka 1.5418 Å radiation and Ni-filter with 2 $\theta$  from 18° to 60°.

### 2.9. Statistical analysis

Data are expressed as means  $\pm$  standard deviations (SD) values from at least two experiments. The significance levels (*p*-values) are calculated using the *t*-test by MedCalc Software for multiple comparisons. Differences in the variables are considered significant at *p* < 0.05 and specified in corresponding figures.

## 3. Results and discussion

### 3.1. Fabrication of CaCO<sub>3</sub>-mucin hybrids

Pure CaCO<sub>3</sub> microcrystals (diameter of 5–6  $\mu$ m) synthesized in this study do not possess high surface charge ( $\zeta$ -potential of 9  $\pm$  2 mV) that is in a good agreement with previous reports [15,40]. Their capacity for the DOX is rather low (average content of 0.11 mg g<sup>-1</sup> CaCO<sub>3</sub>). One

can assume that the loading capacity of the crystals for DOX or other relevant drugs may be enhanced if the crystals are also loaded with a component that can strongly interact with the drugs. This is further investigated here using glycoprotein mucin as a matrix to host DOX and/or other drugs. Being the major component of the mucus, mucin seems to serve as an appropriate constituent element for mucosal drug delivery system. In addition, a number of various interactions (electrostatics, hydrophobic interactions, and hydrogen bonding) attributed to mucin also makes this glycoprotein favorable candidate for the formation of drug-binding polymer matrix. The structure of DOX displays the only one changed group (primary amino group) that may drive electrostatic attraction to sialic acid in mucin (Fig. 1) and hydrophobic anthracycline core tending to hydrophobic interaction with cysteine-rich domains.

Hybrid CaCO<sub>3</sub>-mucin crystals have been prepared by co-synthesis. Mucin has been added to solution of CaCl<sub>2</sub> followed by addition of Na<sub>2</sub>CO<sub>3</sub> during intensive stirring that results in the growth of vaterite crystals containing embedded mucin molecules (Fig. 2, 1). DOX-containing hybrids have been synthesized by simultaneous addition of DOX and mucin during the synthesis as shown in the scheme.

It is known that the concentration of mucin plays a key role in aggregation of mucin molecules and gelation of mucin solution as a result of the aggregation [56]. One can assume that the concentration of mucin during the co-synthesis may affect the structure and properties of the finally formed crystals. First we have evaluated how much of mucin can be loaded into the crystals as a function of initial mucin concentration during the co-synthesis process. Fig. 3 shows the adsorption isotherm for mucin loading.

The results presented in Fig. 3 have been fitted by the classical equation for the Langmuir adsorption model (Eq. (3)). The linearization of the adsorption isotherm in double reciprocal, i.e.  $1/q_e = f(1/C_e)$ , allows one to receive both  $q_{max} = 588 \pm 35$  mg g<sup>-1</sup> and  $K_a = 0.50$  mL mg<sup>-1</sup> ( $R^2$  0.992). These thermodynamic parameters are 3.7 and 5 times higher than those obtained for adsorption of mucin into pre-formed vaterite crystals [40]. We assume that much higher loading of mucin via the co-synthesis than that for the adsorption can be explained by the aggregation of mucin molecules inside the pores of the crystals during the crystal growth. Similar loading mechanism has been proposed for the protein catalase that has been loaded into the crystals in enormous amounts giving the concentration of the protein inside the crystals of >200 mg mL<sup>-1</sup> [29]. We assume that mucin can be loaded at even larger amounts only due to the formation of a mucin hydrogel inside the crystal pores.

Interestingly, the free Gibbs energy change calculated for the loading of mucin via the co-synthesis ( $-31 \pm 3$  kJ mol<sup>-1</sup>) is slightly higher than that obtained for the mucin loading via adsorption onto performed crystals ( $-35 \pm 4$  kJ mol<sup>-1</sup>) [40]. This can likely be caused by the presence of intermolecular interactions between mucin molecules for the loading by the co-synthesis. These interactions may be less favorable than those between crystals surface and mucin because of potential release of water molecules in the case of mucin adsorption on the surface. Intermolecular mucin-mucin interactions result in formation of highly hydrated hydrogel. Nevertheless, rather low  $\Delta G$  indicates a strong affinity of mucin to the crystals for the co-synthesis.

$\zeta$ -potential measurements have proven the presence of mucin on the surface of the crystals. Hybrid crystals have the  $\zeta$ -potential of  $-(8 \pm 2)$  mV, whereas bare crystals are positively charged having the  $\zeta$ -potential of  $+(9 \pm 2)$  mV and mucin is negatively charged in aqueous solution giving the  $\zeta$ -potential of  $-(15 \pm 2)$  mV. The inversion of the  $\zeta$ -potential sign of the surface for mucin-containing hybrids indicates recharging of the crystal surface and an integration of mucin into the crystals.

The morphology of mucin-containing crystals has been assessed using SEM. Fig. 4 shows images of bare crystals (a, c) and those prepared with mucin at highest glycoprotein concentration used, i.e. 6 mg mL<sup>-1</sup> (Fig. 4b, d). The average diameter of the crystals has been increased in

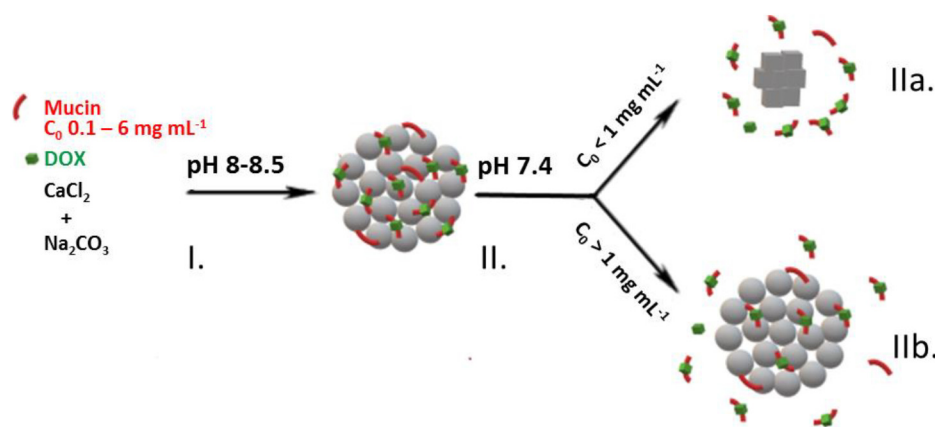


**Fig. 2.** Schematic illustration of (I) the co-synthesis of CaCO<sub>3</sub>-mucin hybrid crystals containing DOX and (II) the release of DOX at physiological conditions via diffusion of mucin-DOX complex out due to recrystallization of the CaCO<sub>3</sub> crystals to calcite (IIa) and the complex diffusion out of the pores of the vaterite crystals (IIb).

the presence of mucin ( $5.8 \pm 0.7$  and  $3.3 \pm 0.8 \mu\text{m}$  with and without mucin, respectively). At the same time, the surface morphology of the hybrids has been changed (Fig. 4c, d). The vaterite crystals are made of small spherical nanocrystals, so called nanocrystallines [15]. SEM images indicate that the size of nanocrystallines for hybrids is significantly smaller than that for bare crystals. The analysis of the crystal surface morphology has revealed average sizes of the nanocrystallines of  $109 \pm 25$  and  $47 \pm 7$  nm for bare crystals and hybrids, respectively (Fig. 4e, f). The direct assessment of the porosity of hybrid mucin-containing crystals via Brunauer-Emmett-Teller surface area analysis is limited due to relatively low thermal stability of mucin that partially decomposes already at  $60^\circ\text{C}$  [57]. However, referring to the morphological analysis of the vaterite crystals that directly correlates the outer surface morphology with the internal structure of the crystals [15], the results above allow one to conclude that the internal structure of the hybrids is likely more developed, i.e. has smaller pores and a larger surface area. Using the inverse relationship between nanocrystalline radii and total surface area of spherical crystals derived in [15] and based on Ostwald ripening mechanism of crystal growth, it is possible to estimate that hybrid crystals possess roughly 2.3 times larger area for hosting molecules.

More porous structure of the hybrids provides excellent perspectives to better retain the loaded mucin as well as other drugs to be co-loaded via co-synthesis, for instance DOX and APR as discussed in the following section.

Solid samples of CaCO<sub>3</sub> and hybrid crystals have shown similar pattern of FTIR spectra (Fig. 5) for which characteristic peaks of the carbonate (broad peak at about  $1300\text{--}1400\text{ cm}^{-1}$ ) and in particular vaterite polymorph of CaCO<sub>3</sub> ( $747, 876\text{ cm}^{-1}$  [58]) have been dominating. No

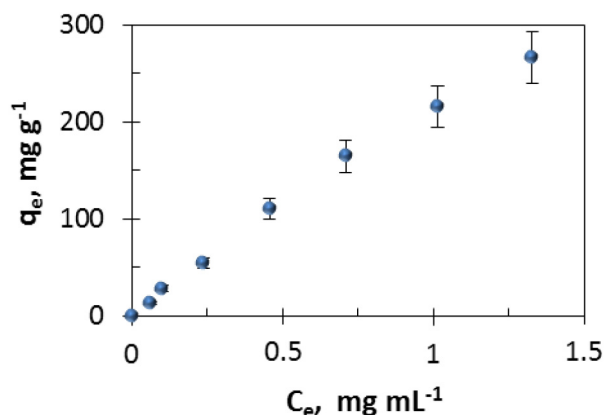


**Fig. 3.** Adsorption isotherm for mucin loading into vaterite CaCO<sub>3</sub> crystals by co-synthesis.

shifts of the bands indicating the recrystallization of vaterite to calcite in the presence of mucin have been detected; the crystals are pure vaterite polymorph. In hybrid crystals, no appearance of characteristic bands of mucin has been detected that might be related to low signal to noise ratio of characteristic amide bonds to CaCO<sub>3</sub> background that is below detection limit.

### 3.2. CaCO<sub>3</sub>-mucin-drug hybrids

In this part of the work the use of co-synthesis for the fabrication of CaCO<sub>3</sub>-based drug delivery carriers for rather small drugs of different nature is examined. For this, three well-known therapeutic drugs have been chosen: DOX (small antibiotic of a molecular mass below 1 kDa) and two protein-based drugs with different net charge, i.e. protease inhibitor aprotinin (APR) and a hormone insulin (INS). Physical-chemical properties of the drugs are summarized in the Table 1 below. Two protein-based drugs with different net charges have been chosen to assess the contribution of electrostatic interactions for rather small drugs of defined dimensions and charges.

Isoelectric point of mucin is in the range of 3–4 and thus glycoprotein possesses a negative charge at the physiologically relevant pH 7.4. This provides an opportunity to form interactions with other substances not only through hydrogen bonding and hydrophobic interactions but also via rather strong coulombic interactions (Fig. 1).

The loading of drugs into CaCO<sub>3</sub>-mucin-drug hybrids has been performed in the presence of 30 mM TRIS buffer (pH 7.1) to ensure that the final pH during the co-synthesis is in the range 8.0–8.5. This pH is considerably lower than that for the co-synthesis in water (pH of about 10.3). Lower pH is beneficial since it would provide milder conditions for loading of protein-based drugs since the majority of labile proteins are pH-sensitive and highly alkaline pH may be harmful for them [62].

Fig. 6 shows the loading efficiency and the amount of released drug for the co-synthesis in the absence (CaCO<sub>3</sub>-drug) and the presence of mucin (CaCO<sub>3</sub>-mucin-drug). The efficiencies for loading of DOX and APR are significantly lower than that for INS (Fig. 6a) which is likely caused by electrostatic attraction of negatively charged INS to positively charged crystals. Inclusion of mucin matrix yields the negative charge to hybrid crystals provoking slight reduction in INS entrapment efficiency.

On the contrary, both DOX and APR possess positive net charge in the pH range of 8.0–8.5 and prone to electrostatic repulsion with positively charged CaCO<sub>3</sub> crystals. The presence of mucin in the hybrid crystals significantly enhances the loading capacity for DOX and APR (Fig. 6a) by 3–5 times (compared to that with no mucin).

The release of the encapsulated drugs (Fig. 6b) supports the hypothesis above. The same amount of INS is released from mucin-containing hybrids and mucin-free crystals proving that the presence of mucin

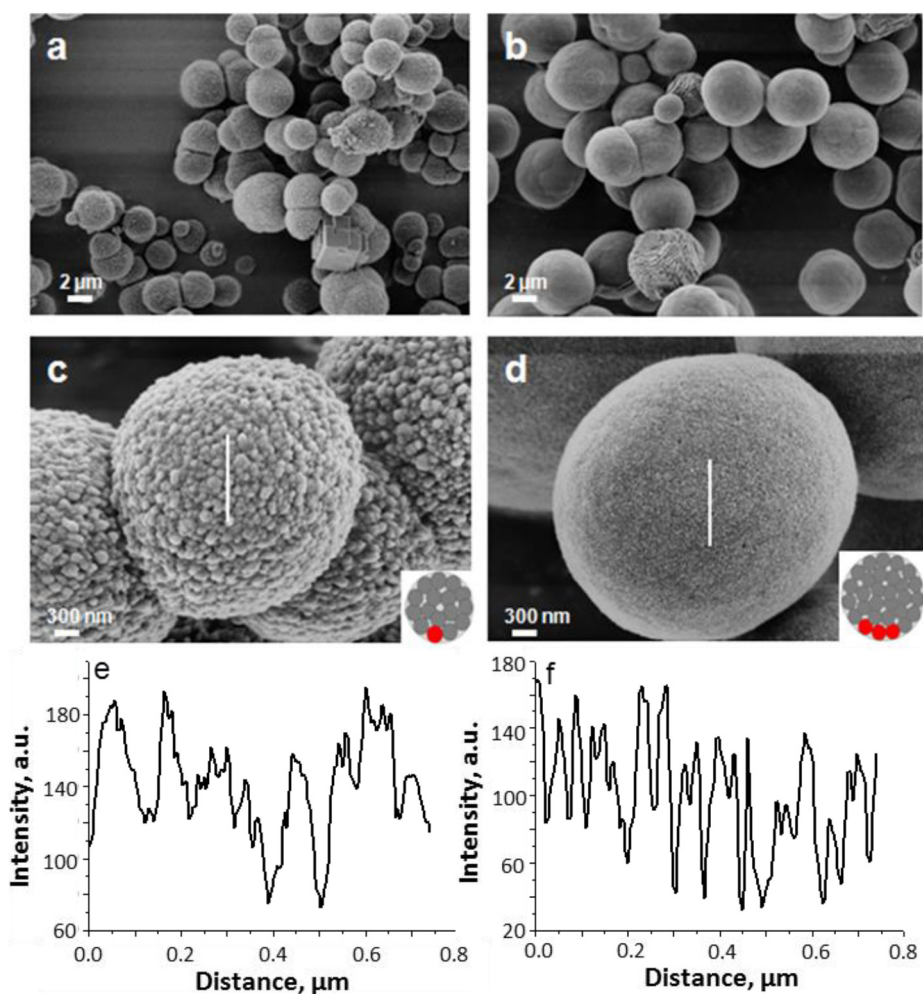


**Fig. 4.** SEM images of pure vaterite crystals (a,c) and those prepared with mucin via co-synthesis (b,d). Profiles (e) and (f) are taken along the white solid lines on the crystal surfaces, to demonstrate a variation of a surface roughness in (c) and (d), respectively. Mucin concentration during the co-synthesis is  $6 \text{ mg mL}^{-1}$ .

does not affect INS interaction with the crystals. At the same time, amounts of DOX and APR released from mucin-containing crystals are almost twice lower than those released from mucin-free crystals, this difference is statistically significant for APR and has a high level of significance ( $p = 0.06$ ) for DOX.

XRD pattern of hybrid  $\text{CaCO}_3$  crystals obtained in the presence of mucin or mucin-DOX has been compared with vaterite synthesized without any additives (Fig. 7). The powder XRD exhibits the characteristic reflections of vaterite with dominant lattice planes of (004), (110), (112), (114), (300) and (118) and less intensive (205), (008), (304) and (224) calculated for the hexagonal cell with  $a = b = 7.169 \text{ \AA}$  and  $c = 16.981 \text{ \AA}$  [63,64]. A negligible peak at  $29.2^\circ$  corresponding to rhombohedral calcite structure also has been detected. No difference in relative Bragg peak intensities (the same XRD pattern) for pure and hybrid crystals points on the absence of morphological changes in the presence of mucin and mucin-DOX that is in agreement with the results of FTIR (Fig. 5). Small broadening of the peaks (an increase in FWHM of 11–17% as calculated for characteristic peaks of 224, 118 and 300) indicate slight decrease in nanocrystalline size that collaborates with SEM (Fig. 4). Significant decrease in the intensity of vaterite observed in the presence of mucin or mucin-DOX is due to the shielding effect of amorphous mucin coating that is indicative for the inclusion of mucin and mucin-DOX in non-crystalline state. Finally, characteristic peaks of mucin (diffraction peaks at  $31.3^\circ$  and  $45.2^\circ$ ) or DOX (multiple peaks appearing within diffraction angle of  $10\text{--}20^\circ$ ) have not been found also indicating the entrapment of amorphous mucin and mucin-DOX complex.

In order to better understand the interaction of mucin and the drugs, analysis of the mucin-drug complex has been done for DOX as described in the following section.

### 3.3. Analysis of the complex mucin-DOX

The complexation between DOX and mucin has been probed by ATR-FTIR spectroscopy. Characteristic bands of functional groups are typically assessed focusing on the wavelength of the band as well as on the shape and the width [55,65,66]. Overlapping of characteristic bands limits proper analysis of the complexation between mucin and APR as well as mucin and INS since all of these substances contain peptide bonds with characteristic Amide I, II, and III bands. At the same time, the overlapping of characteristic bands of mucin (Fig. 8) and DOX (Fig. S1) is not significant.

Interaction between DOX and mucin has been probed via two experiments. In the first experiment, the concentration of mucin was kept constant ( $3 \text{ mg mL}^{-1}$ ) and DOX concentration has been varied in the range of  $0.01\text{--}0.2 \text{ mg mL}^{-1}$  (Fig. 9a). As a negative control for this, the solutions of DOX of varied concentrations have been used.

Mucin contains many C-O-C bonds with the characteristic absorption band of  $1060\text{--}1090 \text{ cm}^{-1}$  (Fig. 8) [66]. The increase of the concentration of DOX at a fixed concentration of mucin resulted in the increase of the intensity of this band as shown in Fig. 9a. After the critical concentration of DOX of  $>0.05 \text{ mg mL}^{-1}$ , the value of the peak intensity has reached a plateau. It is of note that the DOX also contains a sugar moiety as mucin but its contribution to the measured spectra has been

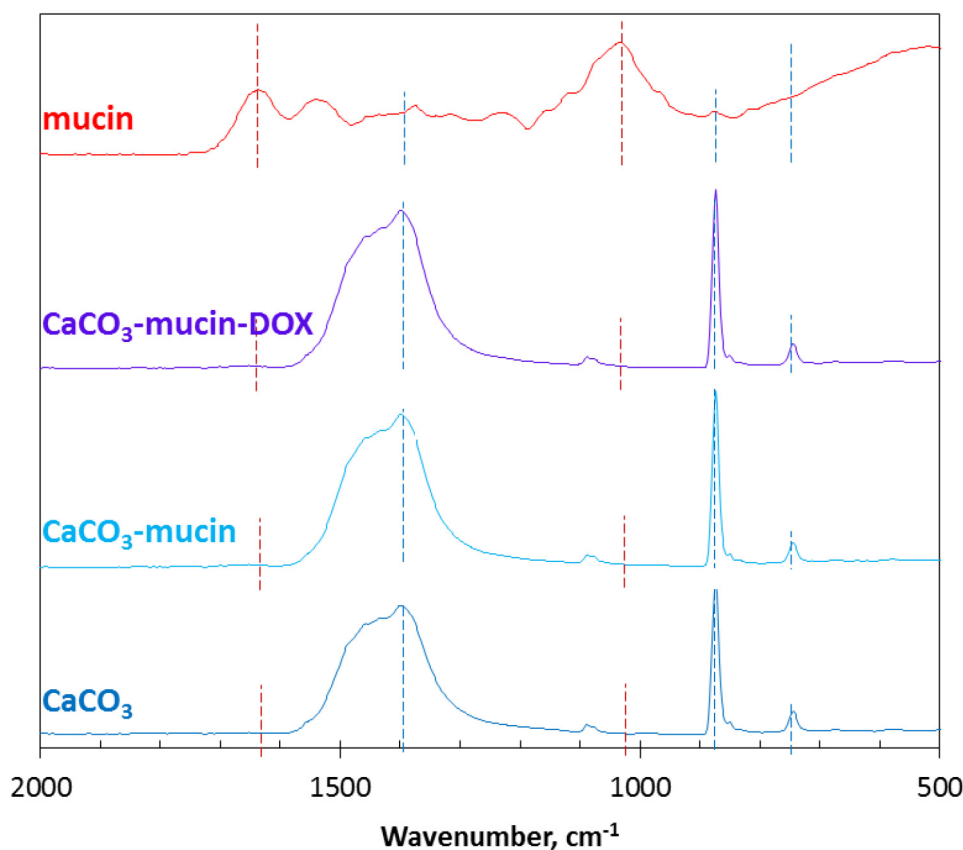


**Fig. 5.** Normalized solid-phase FTIR absorbance spectra of (a) mucin, (b)  $\text{CaCO}_3$ , (c)  $\text{CaCO}_3$ -mucin and (d)  $\text{CaCO}_3$ -mucin-DOX hybrids. Mucin and DOX have been loaded in terms of co-synthesis (initial concentrations during loading were  $4 \text{ mg mL}^{-1}$  for mucin and  $0.1 \text{ mg mL}^{-1}$  for DOX).

subtracted. We assume that the increase of the intensity can be associated with a change of the microenvironment of pyranose cycles in mucin as has been reported in the following works [55,67]. One can assume that these changes are mediated by noncovalent interactions between aromatic rings of DOX and sugar moieties [68]. However, at the point of reaching the plateau, the molar ratio between the DOX and pyranose cycles of mucin molecules is roughly 1:100. In other words, about only one DOX molecule per 100 sugar moieties of mucin molecules induces significant changes in the local microenvironment of mucin. Since this ratio of 1:100 is rather low, it can be assumed that carbohydrate-aromatic interactions are influenced not via direct monosaccharide-anthracycline binding but via electrostatic interaction between carboxylic groups in sialic acid residues of mucin and amino groups of DOX. In the structure of DOX, the amino group is covalently bound to the pyranose cycle, so the interaction of the amino group with the carboxylic group would result in changes in the microenvironment of the pyranose cycle of DOX and consequently affect carbohydrate-aromatic interactions. At the point of reaching the plateau in Fig. 9a (DOX concentration of  $0.05 \text{ mg mL}^{-1}$ ), the molar ratio between DOX and sialic acid residues of mucin molecules (content of around 2.3%) is roughly 1:2.

**Table 1**

Physical-chemical characteristics of the drugs used in this study for loading into  $\text{CaCO}_3$ -mucin-drug hybrids via co-synthesis.  $D_h$  - Hydrodynamic diameter.

Drug	Bio-function	MW, Da	pI	$D_h$ , nm	Ref.
DOX	Anticancer drug	544	8.6	0.5	[59]
APR	Protein-based protease inhibitor	6500	10.5	2.9	[60]
INS	Hormone	5800	5.3	2.7 (monomer) 5,1 (hexamer)	[61]

Electrostatic attraction between  $\text{NH}_2$  and carboxylic group of sialic acid has further been corroborated by the second ATR-FTIR experiment. Deprotonation of the carboxylic group and formation of the  $\text{COO}^-$  ion that has a characteristic band in  $1330\text{--}1390 \text{ cm}^{-1}$  [69] has been detected (Fig. 9b). It is of note that the characteristic band of the  $\text{CH}_2$  group may be found nearby the band for the  $\text{COO}^-$  group, however, these peaks are easy to distinguish by their intensities and half-widths. For instance, the peaks of  $\text{CH}_2$  (deform.) are usually rather wide and have low intensities (for the polymers that are not enriched with  $\text{CH}_2$  groups) while the peaks of the carboxylic group are typically narrow. Moreover, the deformation oscillations usually have less intensity of peaks and are typically less used in the analysis.

The concentration of mucin has been varied in the range of  $2\text{--}4 \text{ mg mL}^{-1}$ , while DOX concentration was kept constant for each measurement at  $0.1 \text{ mg mL}^{-1}$  (Fig. S2). The negative control was chosen as for the first experiment above, i.e. the DOX solution of a corresponding concentration. Fig. 9b demonstrates results of this experiment where it is clear that the peak intensity reaches a plateau at the concentration of mucin  $> 3 \text{ mg mL}^{-1}$ . Notably, the plateau in Fig. 9b corresponds to the molar ratio between DOX and sialic acid residues of mucin molecules of 1:1. This reveals the pivotal role of electrostatic interaction in mucin-DOX binding, yet hydrophobic interactions also might have some impact on mucin-DOX binding as it has been previously reported in [40]. This can be associated with the binding to cysteine-rich domain of mucin (Fig. 1), although more detailed study should be performed to justify this in future.

Further we considered an effect of mucin concentration on the loading/release of DOX into/from the hybrids of  $\text{CaCO}_3$ -mucin-DOX.

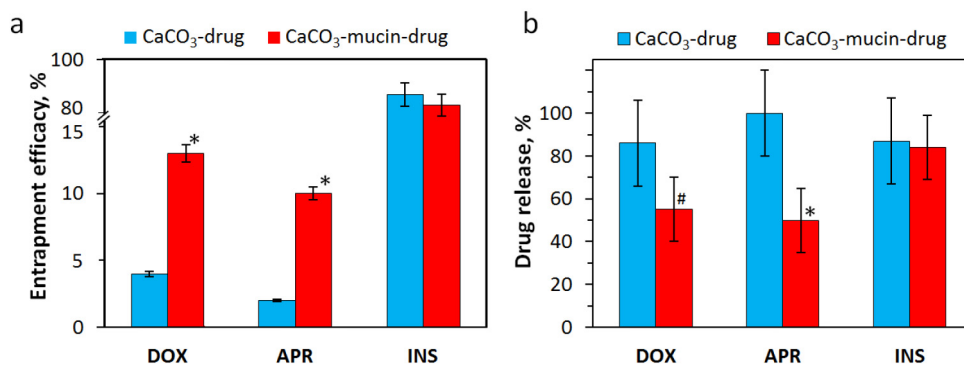


**Fig. 6.** Average drug content per the CaCO<sub>3</sub>-mucin-drug hybrid crystal (a) and the amount of drug released from the hybrids (b). Hybrids are prepared by co-synthesis at the concentrations of mucin and drugs of 1 mg mL<sup>-1</sup> (only for DOX the concentration is 0.1 mg mL<sup>-1</sup>). The release of the drugs from the hybrids is carryout out in 50 mM TRIS buffer, pH 7.4, 24 h incubation. *p*-Values are obtained by comparison of groups indicated: \* *p* < 0.02; # *p* = 0.06.

### 3.4. DOX release from hybrids

First, the influence of mucin concentration at co-synthesis on the loading of DOX into the hybrids has been investigated (Fig. 10). It has been observed that the higher is the concentration of the used mucin, the higher is the amount of the loaded DOX. Notably, the amount of the DOX loaded into the crystals is at least one order of magnitude higher in the presence of mucin compared to the bare crystal. Encapsulation efficiencies ( $\eta$ ) reached via entrapment to CaCO<sub>3</sub>-mucin-DOX hybrid crystals (Fig. 10a) are comparable with those for other DOX delivery systems, e.g. polymeric micelles ( $\eta$  of ca 30%) [70] or hydrogels ( $\eta$  20–40%) [71]. Suspension of the crystals loaded with DOX become coloured as can be clearly observed visually (Fig. S3). This was the case after double washing of the crystals indicating a strong binding of DOX to the hybrid crystals.

At the next step, release mechanism and kinetics have been investigated. Obviously, mucosa of different organs has different environment that also might differ in healthy and pathological tissues that might seriously affect the release profiles. In this study, we have focused on DOX release at pH 7.4 that is relevant to some important clinical cases (Table S1).

First, an effect of the initial mucin concentration on the release of DOX from the hybrids at physiologically relevant conditions has been analyzed. Simultaneous assessment of DOX and mucin release has been performed in order to conclude whether the mucin and DOX

releases are dependent processes. Fig. 11 presents both the relative amount of mucin and DOX released after incubation of the hybrids in TRIS (37 °C) for 24 h. This analysis has been accompanied by the investigation of the morphology of the crystals. The content of spherical vaterite crystals and more thermodynamically stable polymorph of cubic calcite crystals has been identified (Fig. 11, upper panel). Higher concentration of mucin used for the fabrication of hybrid crystals resulted in deceleration of the release for both mucin and DOX; this has been accompanied by an increase of the content of vaterite over calcite polymorph as recorded at 24 h of incubation. The crystals prepared without mucin have been completely recrystallized to calcite and released almost all DOX after 24 h. In contrast, the hybrid crystals with the highest content of mucin used (4 mg mL<sup>-1</sup> concentration during the co-synthesis) have not been recrystallized at all and kept their vaterite structure, releasing only about a third of the loaded mucin and DOX (Fig. 11). This indicates a strong influence of mucin on both the recrystallization of vaterite to calcite and on the rate of DOX release rate. Mucin inhibits recrystallization process that may be caused by hindering the ion transport (Ca<sup>2+</sup> and CO<sub>3</sub><sup>2-</sup>) from the crystal surface due to binding to mucin (recrystallization is the solution-mediated process [72]).

Another interesting finding is that at the tested conditions the amounts of released DOX and mucin are rather similar. This indicates that DOX is released as a complex with mucin. Taking into account the results of ATR-FTIR study described above, it is reasonable to assume

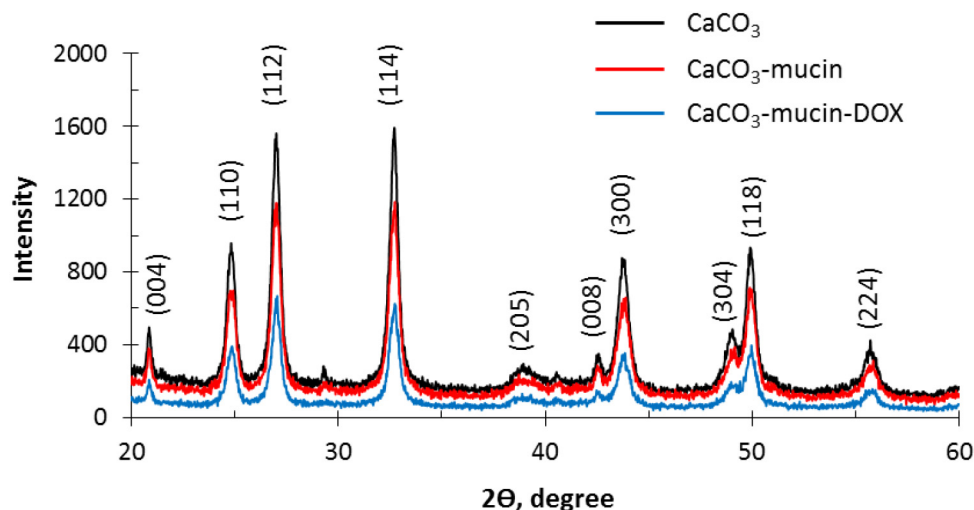


**Fig. 7.** XRD pattern of CaCO<sub>3</sub>, CaCO<sub>3</sub>-mucin and CaCO<sub>3</sub>-mucin-DOX hybrids. Mucin and DOX have been loaded in terms of co-synthesis (initial concentrations during loading were 4 mg mL<sup>-1</sup> for mucin and 0.1 mg mL<sup>-1</sup> for DOX).

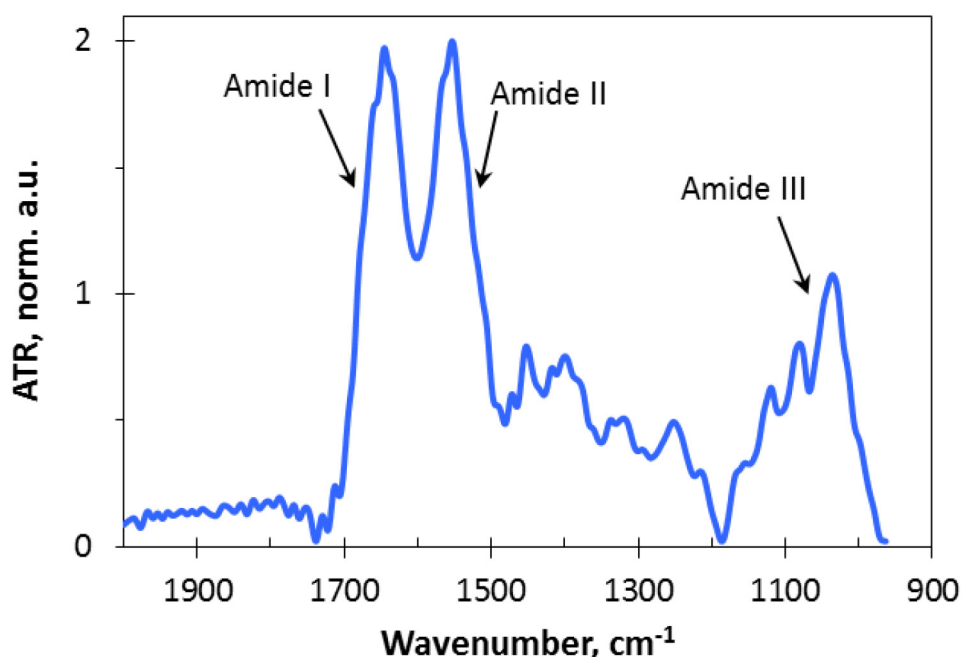


Fig. 8. Normalized FTIR spectrum of mucin (3 mg mL<sup>-1</sup>, 30 mM TRIS buffer pH 7.1, 22 °C).

that DOX in the hybrids is present as a complex with mucin and is released as a complex as well. Moreover, the release rate is dependent on the polymorph state of the crystals. The substantial release of the encapsulated components takes place as soon as the vaterite polymorph is transferred to thermodynamically more stable calcite. Due to non-porous structure of the calcite, the content of the crystals (both mucin and DOX) will release out.

Consequently, the kinetics of DOX release from the hybrids has been investigated. Fig. 11 shows the relative amount of the released DOX as a function of time for the release experiment in 50 mM TRIS buffer, pH 7.4. The release kinetics shows a burst within 1 h followed by a very slow sustained release up to approximately 6 h. At this time point, about 90% of DOX has been released from bare crystals fabricated without mucin while only ca. 30% of DOX has been liberated from hybrid crystals fabricated using mucin concentration of 1–4 mg mL<sup>-1</sup>. The ratio of the released drug from the crystals prepared with/without mucin has been significantly changed after 24 h demonstrating an increase of the released amount of DOX from the hybrid crystals. Herein, higher mucin concentration suppresses the release rate. Longer-term release of DOX (after 24 h) has not been considered in this study and should be described in future works.

These results, considered together with the results in Fig. 11, obviously demonstrate that the recrystallization of vaterite to calcite plays a crucial role in the release kinetics. Non-porous calcite crystals cannot provide enough surface area to host DOX and mucin, the recrystallization results in a substantial release of both components of the hybrids. Of note, mucin and DOX are released dependently (Fig. 11) and one can reasonably assume that the release of mucin is primary important to control the release rate of DOX since DOX is bound to mucin as shown in the ATR-FTIR study above. The strong effect of the recrystallization on the released amount of the encapsulated cargo has been shown previously [26] and the results shown in the Fig. 12 proves that the change in the porosity of vaterite and calcite polymorphs can effectively be used to control the release of substances pre-encapsulated into the vaterite CaCO<sub>3</sub> crystals.

Our preliminary *in vitro* experiments have demonstrated the efficient uptake of CaCO<sub>3</sub> crystals by HepG2 and SK-Hep-1 human liver cancer cells. Moreover, filling of CaCO<sub>3</sub> crystals with carboxymethyl-dextran and formation of model negatively charged macromolecular matrix inside the crystals improved cellular uptake (data are not shown). This is promising indicator for our upcoming *in vitro* study, where the questions of the mechanisms of cellular uptake and intracellular drug release are addressed.

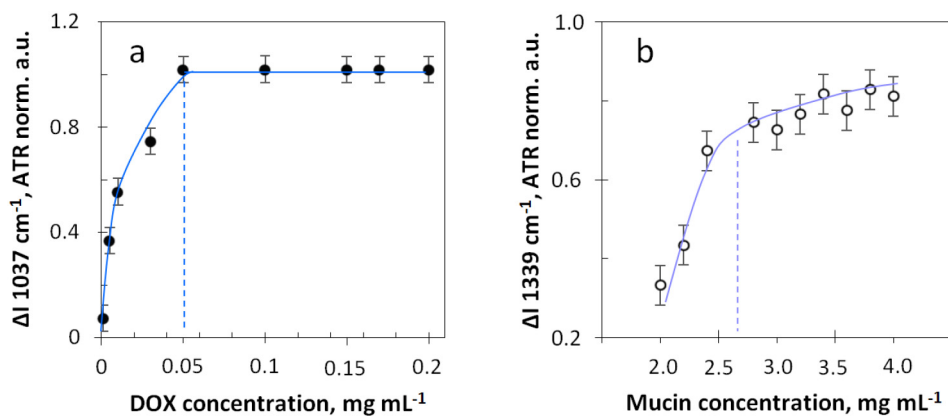


Fig. 9. The dependence of the intensity of the bands 1037 cm<sup>-1</sup> corresponding to C-O-C oscillations and 1339 cm<sup>-1</sup> corresponding to COO<sup>-</sup> oscillations of mucin on: (a) - varied concentration of DOX and the constant concentration of mucin (3 mg mL<sup>-1</sup>) or (b) - varied concentration of mucin and the constant concentration of DOX (0.1 mg mL<sup>-1</sup>). 30 mM TRIS buffer solution, pH 7.1, 22 °C.

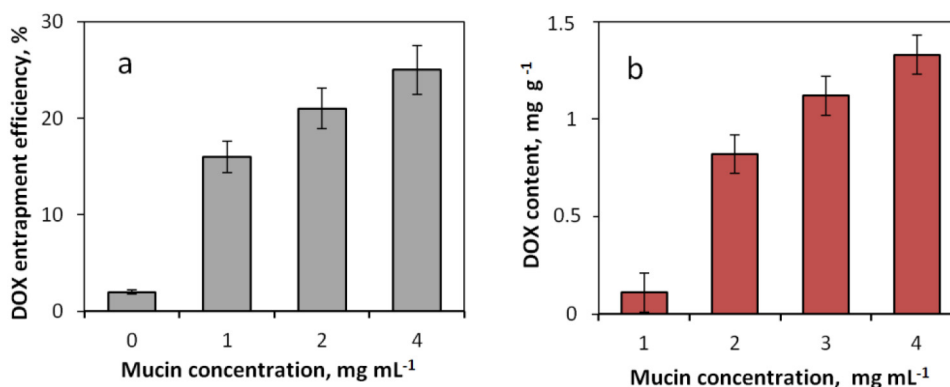


Fig. 10. The average entrapment efficiency (a) and DOX content (b) in CaCO<sub>3</sub>-mucin-DOX hybrid crystal as a function of mucin concentration ( $C_0$ ) during co-synthesis.

#### 4. Conclusions

This study demonstrates that co-synthesis of the anticancer drug DOX and mucin can significantly improve DOX loading (by at least ten times providing concentration of 1.33 mg mL<sup>-1</sup> DOX inside the crystals) and offer a control over the drug release rate from the crystals. Here-with, the content of mucin in the hybrid crystals can reach extremely high value (adsorption capacity of 588 ± 35 mg g<sup>-1</sup>) that exceeds the maximal values possible to be obtained in the solution indicating the formation of a gel in the crystal pores. Mucin binding to the crystals during co-synthesis is strong giving  $K_a$  of 0.50 mL mg<sup>-1</sup> and the free Gibbs

energy change of  $-31 \pm 3$  kJ mol<sup>-1</sup>. DOX is bound preferentially by electrostatic attraction of its amino group to carboxylic groups of mucin as has been proven employing ATR-FTIR spectroscopy. The presence of mucin results in the reduction of pore sizes of the vaterite crystals that taken together with the crystals recrystallization to non-porous calcite polymorph, suppresses DOX release at physiologically relevant conditions. The DOX release is bimodal starting with a burst of ca 1 h, followed by a sustained release within the time scale of tens of hours. This study opens a new avenue for encapsulation and controlled release of small hydrophilic drugs towards applications in mucosal delivery since mucin is a main component of the mucosa and is shown here to

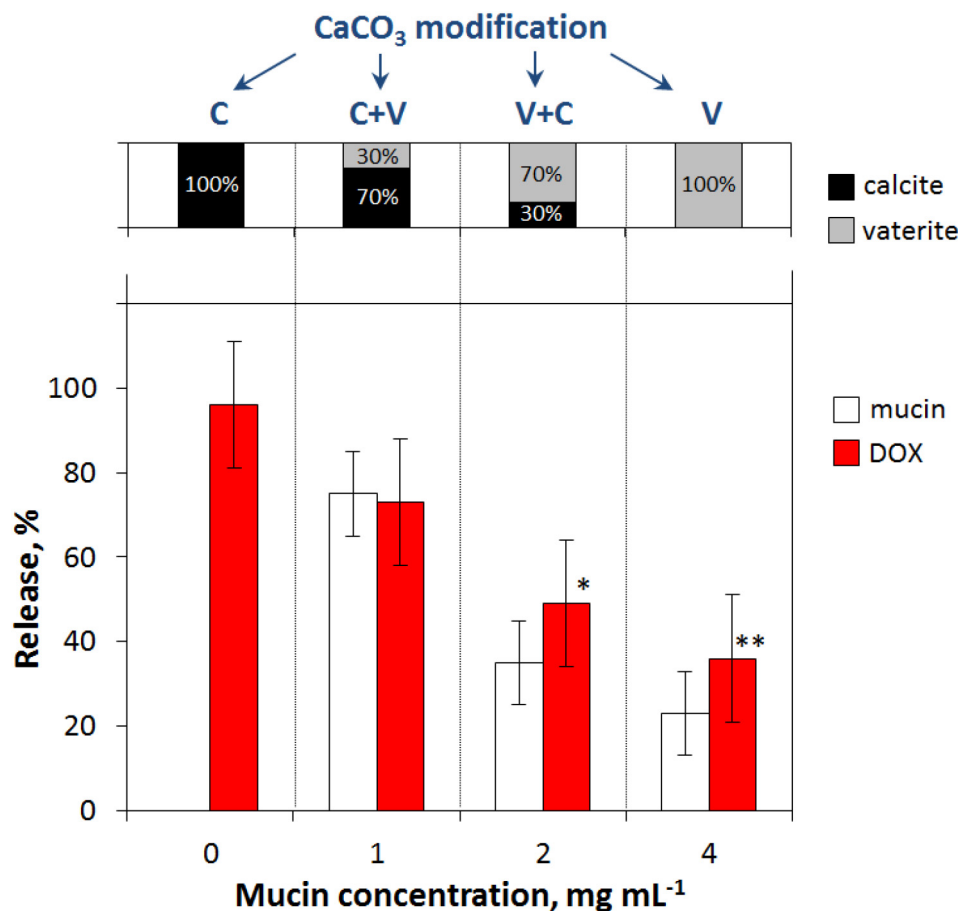
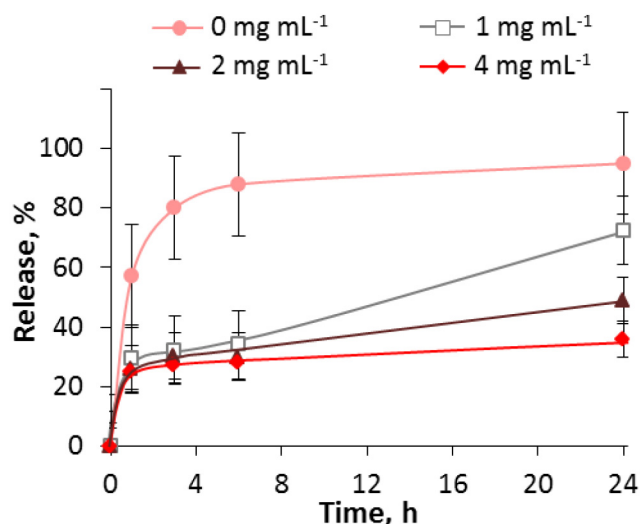


Fig. 11. The influence of the mucin concentration set during the co-synthesis on the relative amount of release DOX and mucin (in % of encapsulated into hybrids) and the dominating presence of vaterite (V) or/and calcite (C) polymorph. The release is assessed after 24 h of incubation in 50 mM TRIS buffer, pH 7.4. C + V and V + C demonstrate dominating of the calcite and vaterite polymorphs, respectively. Pre-loaded amount of DOX (red) or mucin (white) has been taken as 100%.  $p$ -values were obtained by comparison of groups with control (0 mg mL<sup>-1</sup> mucin): \* $p = 0.05$ ; \*\* $p = 0.03$ . (For interpretation of the references to colour in this figure legend, the reader is referred to the web version of this article.)



**Fig. 12.** Kinetics of release of DOX from CaCO<sub>3</sub>-mucin-DOX hybrids in 50 mM TRIS buffer, pH 7.4 for different mucin concentrations used during co-synthesis of the hybrid crystals. Pre-loaded amount of DOX has been taken as 100%.

play a crucial role for drug loading and release. We have demonstrated that the concentration of mucin used during the co-synthesis can significantly affect the DOX release performance and thus can be used for pre-programming and control over the drug release. The pivotal role of electrostatic interaction between mucin and the drugs is supported by probing the binding of DOX (pKa 8.6) and two small protein-based drugs, i.e. APR (pI 10.5) and INS (pI 5.3). DOX is released as a complex with mucin due to a strong interaction driven by Coulomb attractive forces. Moreover, the release strongly depends on the polymorph state of the crystals: the increase of the mucin content in the hybrids reduces the DOX release rate via stabilization of the porous vaterite crystals against recrystallization to non-porous calcite. In addition, the presence of mucin reduces the crystal pore size that makes crystals more capable for the DOX loading and may be used to adjust the DOX release rate.

This study of the growth of vaterite microcrystals in the presence of mucin might contribute to a better understanding of the processes of biomineralization of calcium carbonate, that typically plays a pivotal role in crystallization during the pathological formation of calculus in organs internally covered with mucous membrane. Vaterite crystals which are crystallized in the presence of high mucin concentrations corresponding to those in mucus, better retain cationic bioactives and possess substantial stability under physiological conditions that makes them promising candidates for mucosal drug delivery. Filling of porous vaterite crystals with gel-like matrix of mucin might become a simple and powerful approach for the formulation of CaCO<sub>3</sub>-based drug delivery systems.

#### Data availability

The raw/processed data required to reproduce these findings cannot be shared at this time due to technical or time limitations.

#### CRediT authorship contribution statement

**Nadezhda G. Balabushevich:** Data curation, Funding acquisition, Resources, Formal analysis, Methodology, Investigation, Project administration, Supervision, Writing - original draft, Writing - review & editing. **Ekaterina A. Kovalenko:** Investigation, Formal analysis, Methodology, Writing - review & editing. **Irina M. Le-Deygen:** Investigation, Formal analysis, Methodology, Writing - review & editing. **Lyubov Y. Filatova:** Formal analysis, Methodology, Writing - review & editing. **Dmitry Volodkin:** Conceptualization, Data curation, Funding acquisition, Resources, Formal analysis, Methodology, Project administration,

Supervision, Writing - review & editing. **Anna S. Vikulina:** Conceptualization, Formal analysis, Methodology, Project administration, Supervision, Writing - original draft, Writing - review & editing.

#### Declaration of Competing Interest

The authors declare no conflict of interest.

#### Acknowledgements

This work was carried out with the financial support of M.V. Lomonosov Moscow State University (topic AAAA-A16-116052010081-5). This work was supported in part by M.V. Lomonosov Moscow State University Program of Development. A.V. acknowledges the European Union's Horizon 2020 research and innovation programme for the funding (Marie-Curie Individual Fellowship LIGHTOPLEX-747245). D.V. acknowledges the QR Fund from Nottingham Trent University. The authors thank Ms. A. Ferreira and Dr. C. Polytarchou for their support with the cell culture, and Dr. A. Lapshin from Bruker Optics (Moscow) for their help in solid-phase ATR-FTIR.

#### Appendix A. Supplementary data

Supplementary data to this article can be found online at <https://doi.org/10.1016/j.matdes.2019.108020>.

#### References

- [1] S. Maleki Dizaj, M. Barzegar-Jalali, M.H. Zarrintan, K. Adibkia, F. Lotfipour, Calcium carbonate nanoparticles as cancer drug delivery system, *Expert Opin. Drug Delivery* 12 (2015) 1649–1660.
- [2] R. Roth, J. Schoelkopf, J. Huwiler, M. Puchkov, Functionalized calcium carbonate microparticles for the delivery of proteins, *Eur. J. Pharm. Biopharm.* 122 (2018) 96–103.
- [3] A.D. Trofimov, A.A. Ivanova, M.V. Zyuzin, A.S. Timin, Porous inorganic carriers based on silica, calcium carbonate and calcium phosphate for controlled/modulated drug delivery: fresh outlook and future perspectives, *Pharmaceutics* 10 (2018) 167.
- [4] D. Volodkin, CaCO<sub>3</sub> templated micro-beads and -capsules for bioapplications, *Adv. Colloid Interf. Sci.* 207 (2014) 306–324.
- [5] Y.-H. Won, H.S. Jang, D.-W. Chung, L.A. Stanciu, Multifunctional calcium carbonate microparticles: synthesis and biological applications, *J. Mater. Chem.* 20 (2010) 7728.
- [6] N.G. Balabushevich, V.A. Izumrudov, N.I. Larionova, Protein microparticles with controlled stability prepared via layer-by-layer adsorption of biopolyelectrolytes, *Polym. Sci. Ser. A* 54 (2012) 540–551.
- [7] T.N. Borodina, D.B. Trushina, I.V. Marchenko, T.V. Bukreeva, Calcium carbonate-based mucoadhesive microcontainers for intranasal delivery of drugs bypassing the blood-brain barrier, *BioNanoSci* 6 (2016) 261–268.
- [8] T.V. Bukreeva, I.V. Marchenko, T.N. Borodina, I.V. Degtev, S.L. Sitnikov, Y.V. Moiseeva, N.V. Gulyaeva, M.V. Kovalchuk, Calcium carbonate and titanium dioxide particles as a basis for container fabrication for brain delivery of compounds, *Dokl. Phys. Chem.* 440 (2011) 165–167.
- [9] P.V. Binevski, N.G. Balabushevich, V.I. Uvarova, A.S. Vikulina, D. Volodkin, Biofriendly encapsulation of superoxide dismutase into vaterite CaCO<sub>3</sub> crystals. Enzyme activity, release mechanism, and perspectives for ophthalmology, *Colloids Surf., B* 181 (2019) 437–449.
- [10] M. Fujiwara, K. Shiokawa, M. Araki, N. Ashitaka, K. Morigaki, T. Kubota, Y. Nakahara, Encapsulation of proteins into CaCO<sub>3</sub> by phase transition from vaterite to calcite, *Cryst. Growth Des.* 10 (2010) 4030–4037.
- [11] N. Sudareva, H. Popova, N. Saprykina, S. Bronnikov, Structural optimization of calcium carbonate cores as templates for protein encapsulation, *J. Microencapsul.* 31 (2014) 333–343.
- [12] S. Schmidt, K. Uhlig, C. Duschl, D. Volodkin, Stability and cell uptake of calcium carbonate templated insulin microparticles, *Acta Biomater.* 10 (2014) 1423–1430.
- [13] A.S. Vikulina, N.A. Feoktistova, N.G. Balabushevich, A.G. Skirtach, D. Volodkin, The mechanism of catalase loading into porous vaterite CaCO<sub>3</sub> crystals by co-synthesis, *Phys. Chem. Chem. Phys.* 20 (2018) 8822–8831.
- [14] P. Wang, N. Yu, Y. Wang, H. Sun, Z. Yang, S. Zhou, Co-delivery of PLK1-specific shRNA and doxorubicin via core-crosslinked pH-sensitive and redox ultra-sensitive micelles for glioma therapy, *J. Mater. Chem. B* 6 (2018) 112–124.
- [15] N. Feoktistova, J. Rose, V.Z. Prokopović, A.S. Vikulina, A. Skirtach, D. Volodkin, Controlling the vaterite CaCO<sub>3</sub> crystal pores. Design of tailor-made polymer based microcapsules by hard templating, *Langmuir* 32 (2016) 4229–4238.
- [16] B.V. Parakhonskiy, A.M. Yashchenok, S. Donatan, D.V. Volodkin, F. Tessarolo, R. Antolini, H. Möhwald, A.G. Skirtach, Macromolecule loading into spherical, elliptical, star-like and cubic calcium carbonate carriers, *ChemPhysChem* 15 (2014) 2817–2822.

- [17] L. Jeannot, M. Bell, R. Ashwell, D. Volodkin, A. Vikulina, Internal structure of matrix-type multilayer capsules templated on porous vaterite  $\text{CaCO}_3$  crystals as probed by staining with a fluorescence dye, *Micromachines* 9 (2018) 547.
- [18] T. Paulraj, N. Feoktistova, N. Velk, K. Uhlrig, C. Duschl, D. Volodkin, Microporous polymeric 3D scaffolds templated by the layer-by-layer self-assembly, *Macromol. Rapid Commun.* 35 (2014) 1408–1413.
- [19] M.S. Savelyeva, A.A. Abalymov, G.P. Lyubun, I.V. Vidyasheva, A.M. Yashchenok, T.E.L. Douglas, D.A. Gorin, B.V. Parakhonskiy, Vaterite coatings on electrospun polymeric fibers for biomedical applications, *J. Biomed. Mater. Res., Part A* 105 (2017) 94–103.
- [20] T.E.L. Douglas, A. Łapa, S.K. Samal, H.A. Declercq, D. Schaubroeck, A.C. Mendes, P. van der Voort, A. Dokupil, A. Plis, K. de Schampheleere, I.S. Chronakis, E. Pamuła, A.G. Skirtach, Enzymatic, urease-mediated mineralization of gellan gum hydrogel with calcium carbonate, magnesium-enriched calcium carbonate and magnesium carbonate for bone regeneration applications, *J. Tissue Eng. Regen. Med.* 11 (2017) 3556–3566.
- [21] M.A. Lopez-Heredia, A. Łapa, K. Reczyńska, K. Pietryga, L. Balcaen, A.C. Mendes, D. Schaubroeck, P. van der Voort, A. Dokupil, A. Plis, C.V. Stevens, B.V. Parakhonskiy, S.K. Samal, F. Vanhaecke, F. Chai, I.S. Chronakis, N. Blanchemain, E. Pamuła, A.G. Skirtach, T.E.L. Douglas, Mineralization of gellan gum hydrogels with calcium and magnesium carbonates by alternate soaking in solutions of calcium/magnesium and carbonate ion solutions, *J. Tissue Eng. Regen. Med.* 12 (2018) 1825–1834.
- [22] N. Feoktistova, G. Stoychev, N. Pureskiy, L. Ionov, D. Volodkin, Porous thermo-responsive pNIPAM microgels, *Eur. Polym. J.* 68 (2015) 650–656.
- [23] M. Behra, S. Schmidt, J. Hartmann, D.V. Volodkin, L. Hartmann, Synthesis of porous PEG microgels using  $\text{CaCO}_3$  microspheres as hard templates, *Macromol. Rapid Commun.* 33 (2012) 1049–1054.
- [24] I.Y. Stetsiura, A. Yashchenok, A. Masic, E.V. Lyubin, O.A. Inozemtseva, M.G. Drozdova, E.A. Markvichova, B.N. Khebtsov, A.A. Fedyanin, G.B. Sukhorukov, D.A. Gorin, D. Volodkin, Composite SERS-based satellites navigated by optical tweezers for single cell analysis, *Analyst* 140 (2015) 4981–4986.
- [25] I.Y. Stetsiura, A.V. Markin, A.N. Ponomarev, A.V. Yakimansky, T.S. Demina, C. Grandfils, D.V. Volodkin, D.A. Gorin, New surface-enhanced Raman scattering platforms: composite calcium carbonate microspheres coated with astralen and silver nanoparticles, *Langmuir* 29 (2013) 4140–4147.
- [26] A. Sergeeva, R. Sergeev, E. Lengert, A. Zakharevich, B. Parakhonskiy, D. Gorin, S. Sergeev, D. Volodkin, Composite magnetite and protein containing  $\text{CaCO}_3$  crystals. External manipulation and vaterite  $\rightarrow$  calcite recrystallization-mediated release performance, *ACS Appl. Mater. Interfaces* 7 (2015) 21315–21325.
- [27] A. Sergeeva, N. Feoktistova, V. Prokopovic, D. Gorin, D. Volodkin, Design of porous alginate hydrogels by sacrificial  $\text{CaCO}_3$  templates: pore formation mechanism, *Adv. Mater. Interfaces* 2 (2015), 1500386.
- [28] A.S. Sergeeva, D.A. Gorin, D.V. Volodkin, In-situ assembly of Ca-alginate gels with controlled pore loading/release capability, *Langmuir* 31 (2015) 10813–10821.
- [29] N.G. Balabushevich, A.V. Lopez de Guereñu, N.A. Feoktistova, D. Volodkin, Protein loading into porous  $\text{CaCO}_3$  microspheres: adsorption equilibrium and bioactivity retention, *Phys. Chem. Chem. Phys.* 17 (2015) 2523–2530.
- [30] P. Shi, S. Luo, B. Voit, D. Appelhans, X. Zan, A facile and efficient strategy to encapsulate the model basic protein lysozyme into porous  $\text{CaCO}_3$ , *J. Mater. Chem. B* 6 (2018) 4205–4215.
- [31] V.E. Bosio, M.L. Caciccedo, B. Calvignac, I. León, T. Beuving, F. Boury, G.R. Castro, Synthesis and characterization of  $\text{CaCO}_3$ -biopolymer hybrid nanoporous microparticles for controlled release of doxorubicin, *Colloids Surf., B* 123 (2014) 158–169.
- [32] N.A.N. Hanafy, M.L. de Giorgi, C. Nobile, M. Cascione, R. Rinaldi, S. Leporatti,  $\text{CaCO}_3$  rods as chitosan-polygalacturonic acid carriers for bromopyruvic acid delivery, *Sci. Adv. Mater.* 8 (2016) 514–523.
- [33] M.A. Hood, K. Landfester, R. Muñoz-Espí, Chitosan nanoparticles affect polymorph selection in crystallization of calcium carbonate, *Colloids Surf. A Physicochem. Eng. Asp.* 540 (2018) 48–52.
- [34] N.A. Hanafy, E.-K. M. L. S, Optimizing  $\text{CaCO}_3$  matrix might allow to raise their potential use in biomedical application, *J. Nanosci. Curr. Res.* 3 (2018) 124.
- [35] Y. Zhang, L. Cai, Di Li, Y.-H. Lao, D. Liu, M. Li, J. Ding, X. Chen, Tumor microenvironment-responsive hyaluronate-calcium carbonate hybrid nanoparticle enables effective chemotherapy for primary and advanced osteosarcomas, *Nano Res.* 11 (2018) 4806–4822.
- [36] V. Vergaro, P. Papadia, S. Leporatti, S.A. de Pascali, F.P. Fanizzi, G. Ciccarella, Synthesis of biocompatible polymeric nano-capsules based on calcium carbonate: a potential cisplatin delivery system, *J. Inorg. Biochem.* 153 (2015) 284–292.
- [37] N.G. Balabushevich, E.A. Sholina, E.V. Mikhailchik, L.Y. Filatova, A.S. Vikulina, D. Volodkin, Self-assembled mucin-containing microcarriers via hard templating on  $\text{CaCO}_3$  crystals, *Micromachines* 9 (2018) 307.
- [38] R. Bansil, B.S. Turner, The biology of mucus: composition, synthesis and organization, *Adv. Drug Deliv. Rev.* 124 (2018) 3–15.
- [39] J. Dekker, J.W.A. Rossen, H.A. Büller, A.W.C. Einerhand, The MUC family: an obituary, *Trends Biochem. Sci.* 27 (2002) 126–131.
- [40] N.G. Balabushevich, E.A. Kovalenko, E.V. Mikhailchik, L.Y. Filatova, D. Volodkin, A.S. Vikulina, Mucin adsorption on vaterite  $\text{CaCO}_3$  microcrystals for the prediction of mucoadhesive properties, *J. Colloid Interface Sci.* 545 (2019) 330–339.
- [41] J. Wang, W. Xu, S. Li, H. Qiu, Z. Li, C. Wang, X. Wang, J. Ding, Polylactide-cholesterol stereocomplex micelle encapsulating chemotherapeutic agent for improved antitumor efficacy and safety, *J. Biomed. Nanotechnol.* 14 (2018) 2102–2113.
- [42] K. Zhao, Di Li, W. Xu, J. Ding, W. Jiang, M. Li, C. Wang, X. Chen, Targeted hydroxyethyl starch prodrug for inhibiting the growth and metastasis of prostate cancer, *Biomaterials* 116 (2017) 82–94.
- [43] J. Chen, J. Ding, Y. Wang, J. Cheng, S. Ji, X. Zhuang, X. Chen, Sequentially responsive shell-stacked nanoparticles for deep penetration into solid tumors, *Adv. Mater.* 29 (2017), 1701170.
- [44] J. Chen, J. Ding, W. Xu, T. Sun, H. Xiao, X. Zhuang, X. Chen, Receptor and microenvironment dual-recognizable nanogel for targeted chemotherapy of highly metastatic malignancy, *Nano Lett.* 17 (2017) 4526–4533.
- [45] Y. Zhang, F. Wang, M. Li, Z. Yu, R. Qi, J. Ding, Z. Zhang, X. Chen, Self-stabilized hyaluronate nanogel for intracellular codelivery of doxorubicin and cisplatin to osteosarcoma, *Adv. Sci. (Weinheim, Ger.)* 5 (1700821) (2018).
- [46] Y. Zhang, J. Zhang, W. Xu, G. Xiao, J. Ding, X. Chen, Tumor microenvironment-labile polymer-doxorubicin conjugate thermogel combined with docetaxel for in situ synergistic chemotherapy of hepatoma, *Acta Biomater.* 77 (2018) 63–73.
- [47] I. Borišev, J. Mrdanovic, D. Petrovic, M. Seke, D. Jović, B. Srdenović, N. Latinovic, A. Djordjevic, Nanoformulations of doxorubicin: how far have we come and where do we go from here? *Nanotechnology* 29 (2018), 332002.
- [48] S.V. Mussi, G. Perekh, P. Pattekari, T. Levchenko, Y. Lvov, L.A.M. Ferreira, V.P. Torchilin, Improved pharmacokinetics and enhanced tumor growth inhibition using a nanostructured lipid carrier loaded with doxorubicin and modified with a layer-by-layer polyelectrolyte coating, *Int. J. Pharm.* 495 (2015) 186–193.
- [49] W. Ke, Y. Zhao, R. Huang, C. Jiang, Y. Pei, Enhanced oral bioavailability of doxorubicin in a dendrimer drug delivery system, *J. Pharm. Sci.* 97 (2008) 2208–2216.
- [50] P.S. Averin, A.V. Lopes de Gerenyu, N.G. Balabushevich, Polyelectrolyte micro- and nanoparticles with doxorubicin, *Mosc. Univ. Chem. Bull.* 71 (2016) 140–145.
- [51] N.G. Balabushevich, M.A. Pechenkin, I.N. Zorov, E.D. Shibanova, N.I. Larionova, Mucoadhesive polyelectrolyte microparticles containing recombinant human insulin and its analogs aspart and lispro, *Biochemistry. Biokhimiia* 76 (2011) 327–331.
- [52] N.G. Balabushevich, Anna V. Lopez de Guereñu, N.A. Feoktistova, A.G. Skirtach, D. Volodkin, Protein-containing multilayer capsules by templating on mesoporous  $\text{CaCO}_3$  particles: POST- and PRE-loading approaches, *Macromol. Biosci.* 16 (2016) 95–105.
- [53] I.M. Le-Deygen, A.A. Skuredina, I.V. Uporov, E.V. Kudryashova, Thermodynamics and molecular insight in guest-host complexes of fluoroquinolones with  $\beta$ -cyclodextrin derivatives, as revealed by ATR-FTIR spectroscopy and molecular modeling experiments, *Anal. Bioanal. Chem.* 409 (2017) 6451–6462.
- [54] I.M. Deygen, C. Seidl, D.K. Kölmel, C. Bednarek, S. Heissler, E.V. Kudryashova, S. Bräse, U. Schepers, Novel prodrug of doxorubicin modified by stearylpermine encapsulated into PEG-chitosan-stabilized liposomes, *Langmuir* 32 (2016) 10861–10869.
- [55] I.M. Deygen, E.V. Kudryashova, Structure and stability of anionic liposomes complexes with PEG-chitosan branched copolymer, *Russ. J. Bioorg. Chem.* 40 (2014) 547–557.
- [56] R. Bansil, B.S. Turner, Mucin structure, aggregation, physiological functions and biomedical applications, *Curr. Opin. Colloid Interface Sci.* 11 (2006) 164–170.
- [57] N. Barbero, M. Marenchino, R. Campos-Olivas, S. Oliaro-Bosso, L. Bonandini, J. Boskovic, G. Viscardi, S. Visentin, Nanomaterial-protein interactions: the case of pristine and functionalized carbon nanotubes and porcine gastric mucin, *J. Nanopart. Res.* 18 (2016) 164.
- [58] N. Vagenas, Quantitative analysis of synthetic calcium carbonate polymorphs using FT-IR spectroscopy, *Talanta* 59 (2003) 831–836.
- [59] Z. Fülöp, R. Gref, T. Loftsson, A permeation method for detection of self-aggregation of doxorubicin in aqueous environment, *Int. J. Pharm.* 454 (2013) 559–561.
- [60] H. Fritz, G. Wunderer, Biochemistry and applications of aprotinin, the kallikrein inhibitor from bovine organs, *Arzneim. Forsch.* 33 (1983) 479–494.
- [61] J. Brange, D.R. Owens, S. Kang, A. Volund, Monomeric insulins and their experimental and clinical implications, *Diabetes Care* 13 (1990) 923–954.
- [62] T. Hidaka, A. Shimada, Y. Nakata, H. Kodama, H. Kurihara, T. Tokihiro, S. Ihara, Simple model of pH-induced protein denaturation, *Phys. Rev. E* 92 (2015), 12709.
- [63] A.G. Christy, A review of the structures of vaterite: the impossible, the possible, and the likely, *Cryst. Growth Des.* 17 (2017) 3567–3578.
- [64] S. Hayakawa, Y. Hajima, S. Qiao, H. Namatame, T. Hirokawa, Characterization of calcium carbonate polymorphs with Ca K edge X-ray absorption fine structure spectroscopy, *Anal. Sci.* 24 (2008) 835–837.
- [65] I.M. Deygen, E.V. Kudryashova, New versatile approach for analysis of PEG content in conjugates and complexes with biomacromolecules based on FTIR spectroscopy, *Colloids Surf., B* 141 (2016) 36–43.
- [66] E. Goormaghtigh, V. Raussens, J.M. Ruysschaert, Attenuated total reflection infrared spectroscopy of proteins and lipids in biological membranes, *Biochim. Biophys. Acta* 1422 (1999) 105–185.
- [67] S.J. Parikh, J. Chorover, ATR-FTIR spectroscopy reveals bond formation during bacterial adhesion to iron oxide, *Langmuir* 22 (2006) 8492–8500.
- [68] J.L. Asensio, A. Ardá, F.J. Jiménez-Barbero, Carbohydrate-aromatic interactions, *Acc. Chem. Res.* 46 (2013) 946–954.
- [69] S.E. Cabaniss, I.F. McVey, Aqueous infrared carboxylate absorbances: aliphatic monocarboxylates, *Spectrochim. Acta, Part A* 51 (1995) 2385–2395.
- [70] T.A. Debele, K.-Y. Lee, N.-Y. Hsu, Y.-T. Chiang, L.-Y. Yu, Y.-A. Shen, C.-L. Lo, A pH sensitive polymeric micelle for co-delivery of doxorubicin and  $\alpha$ -TOS for colon cancer therapy, *J. Mater. Chem. B* 5 (2017) 5870–5880.
- [71] M. Dadsatan, Z. Liu, M. Pumberger, C.V. Giraldo, T. Ruesink, L. Lu, M.J. Yaszemski, A stimuli-responsive hydrogel for doxorubicin delivery, *Biomaterials* 31 (2010) 8051–8062.
- [72] N.G. Balabushevich, M.A. Pechenkin, E.D. Shibanova, D.V. Volodkin, E.V. Mikhailchik, Multifunctional polyelectrolyte microparticles for oral insulin delivery, *Macromol. Biosci.* 13 (2013) 1379–1388.